SCIENTIFIC REPORTS

OPEN

SUBJECT AREAS:
NANOPARTICLES
COLLOIDS

Received
28 September 2014

Accepted
8 December 2014

Published
8 January 2015

Correspondence and requests for materials should be addressed to Y.L. (yueli@issp.ac.cn)

* These authors contributed equally to this work.

Rapid Synthesis of Monodisperse Au Nanospheres through a Laser Irradiation -Induced Shape Conversion, Self-Assembly and Their Electromagnetic Coupling SERS Enhancement

Dilong Liu[1,2]*, Cuncheng Li[3]*, Fei Zhou[1], Tao Zhang[3], Honghua Zhang[1,2], Xinyang Li[1], Guotao Duan[1], Weiping Cai[1] & Yue Li[1,2]

[1]Key Lab of Materials Physics, Anhui Key Lab of Nanomaterials and Nanotechnology, institute of Solid State Physics, Chinese Academy of Sciences, Hefei 230031, P. R. China, [2]Department of Materials Science & Engineering, University of Science and technology of China, Hefei 230026, P. R. China, [3]Key Laboratory of Chemical Sensing & Analysis in Universities of Shandong (University of Jinan), School of Chemistry and Chemical Engineering, University of Jinan, Jinan 250022, Shandong, P. R. China.

We develop a facile and effective strategy to prepare monodispersed Au spherical nanoparticles by two steps. Large-scale monocrystalline Au nanooctahedra with uniform size were synthesized by a polyol-route and subsequently Au nanoparticles were transformed from octahedron to spherical shape in a liquid under ambient atmosphere by non-focused laser irradiation in very short time. High monodipersed, ultra-smooth gold nanospheres can be obtained by simply optimizing the laser fluence and irradiation time. Photothermal melting-evaporation model was employed to get a better understanding of the morphology transformation for the system of nanosecond pulsed-laser excitation. These Au nanoparticles were fabricated into periodic monolayer arrays by self-assembly utilizing their high monodispersity and perfect spherical shape. Importantly, such Au nanospheres arrays demonstrated very good SERS enhancement related to their periodic structure due to existence of many SERS hot spots between neighboring Au nanospheres caused by the electromagnetic coupling in an array. These gold nanospheres and their self-assembled arrays possess distinct physical and chemical properties. It will make them as an excellent and promising candidate for applying in sensing and spectroscopic enhancement, catalysis, energy, and biology.

Gold nanoparticles have attracted much interest because of their tunable Surface Plasmon Resonance (SPR) peaks, leading to important applications in the fields of chemistry, biology and materials sciences[1–7]. As is well known, the SPR properties of metallic nanoparticles (NPs) can be calculated by solving Maxwell's equations[8] in terms of theory, and exact solutions to Maxwell's equations are known only for spheres, concentric spherical shells, spheroids, and infinite cylinders[9]. Specifically, Mie theory is the exact analytical solution of Maxwell's equations for a nanoparticle with defined shape[10]. However, it is difficult to synthesize monodispersed noble metallic nanoparticles in a wide range of sizes and controlled shapes on a large scale, and their observed optical absorption property can not obey Mie theory prediction accurately.

In recent years, gold spherical nanoparticles have attracted much attention in fundamental research[11,12], such as Fano resonance[13,14]. Since such spherical nanostructures will give precise SPR spectra and can exclude the undesirable SPR signals originating from the particle corner, facets and size distribution in contrast with the arbitrary shape[10,15]. Hence, a gold perfectly spherical nanoparticle is an ideal model to verify the optical property predicted by Mie theory under light irradiation.

More recently, focus has also turned to cellular and medical applications for such gold nanoparticles[2,16]. Besides the effects of size and surface functional group of gold nanoparticles, a particle shape is another important influence for delivering it into the cell[17]. For instance, Chithrani et al. showed that gold nanoparticles with spherical shapes took shorter wrapping time to wrap the entire bulk in comparison to the nanorod because of the decrease in the surface area[18,19]. Therefore it is urgent to obtain the homogeneous gold nanospheres without

any facets. However, the crystalline gold nanoparticles (NPs) prepared in a solution phase always tend to grow anisotropic and accompany with a high tendency to form distinct facets naturally[20,21], driven by the surface free energy minimization[22]. To date, there have many demonstrations focusing on the synthesis of Au nanospheres, such as a citrate reduction method[23,24], Brust−Schiffrin method[25,26], seeding growth method[27,28]. However, most of the nanospheres reported in these methods are not in a truly spherical shape. Usually, they are multiply twinned particles with more or less rounded profile and with smaller facets on the surface[9]. In other words, these nanoparticles obtained by classical growth methods should be called quasi-spheres. It still keeps a challenge to obtain the ultra-smooth gold nanospheres with high monodispersity.

To address this requirement, some investigations have been tried to produce real-nanospheres. These methods can be roughly divided into wet chemical methods and novel physical methods for auxiliary. In wet chemical methods, Lee et al.[22] developed a strategy to prepare ultra-smooth, highly spherical monocrystalline gold particles by using the growth in solution and subsequently chemical etching method. Undeniably, these spherical gold crystals are smoother than the one synthesized by conventional chemical methods. But the etching process only removes selectively the grain edges and boundary which have higher surface free energy. Scrutinizing these particles, one can find that the leaving intact particles still have smaller facets. In physical methods, a laser irradiation has been used to modify varieties of noble metal nanostructure to spherical morphology. Koshizaki's group[29–32] developed a non-focused laser irradiation method to produce spherical sub-micrometer particles of various materials in nanocolloids. In their method, ultra-smooth spherical sub-micrometer particles have been obtained, but display an uncontrollable size distribution, resulting in polydispersity. For contrast, Werner, D. et al.[33] reported that gold nanospheres with controllable size distribution can be fabricated by tuning the adscititious pressure, laser intensity and excitation wavelength in laser irradiation. They emphasized that the application of an external high pressure have suppressed the formation of the bubble, under this case, the size of gold nanospheres can be controlled only by further changing the laser fluence. The application of adscititious pressure makes manipulation in the preparation process complex.

Herein, we develop a facile and effective strategy to achieve monodispersed Au spherical nanoparticles. Firstly, large-scale monocrystalline Au octahedral nanoparticle with uniform size are synthesized by a straightforward polyol-route. The size dimensions of Au octahedra can be manipulated from tens to hundreds of nanometers. Secondly, non-focused laser irradiation technology is applied to transform Au particles from octahedron to spherical shape in a liquid under ambient atmosphere in short time. Ultra-smooth gold nanospheres with high monodispersity can be obtained by simply optimizing the laser fluence and irradiation time. Moreover, the morphology transformation of Au octahedral nanoparticle under the nanosecond laser irradiation strongly depends on a photothermal melting-evaporation process. Further, these Au nanoparticles can be fabricated into ordered arrays by self-assembly technique due to their high monodispersity and perfect spherical shape. Importantly, such Au nanospheres array shows a significantly SERS performance associated with their periodic structure due to existence of many SERS hot spots between neighboring Au nanospheres in an array. These gold nanospheres and their self-assembled arrays possess distinct physical and chemical properties that will make them as an excellent and promising candidate for applying in sensing and spectroscopic enhancement, catalysis, energy, and biology[34–36].

Results

Pristine Au nanoparticle aqueous colloidal solutions obtained by polyol process contain a large amount of Au uniform, highly mono-dispersed octahedral nanoparticles with average edge lengths of 72 (±3.1) nm. It should be mentioned that this edge length is slightly smaller than real one, because the measured value is a horizontal projection of edge length and the vertex of the octahedral nanoparticles is faded out (see Fig. S1 in support information). These nanoparticles were placed under a non-focused nanosecond pulsed laser with wavelength of 532 nm for irradiation using gentle laser fluence at 3.84 mJ cm^{-2} for 60 seconds. Under such optimized experimental condition, a large amount of spherical nanoparticles were produced, as shown in Figure 1. SEM images in Figure 1a and 1b show that these Au NPs exhibit uniform spherical shapes. Corresponding TEM image shown in Figure 1c indicates these Au nanoparticles demonstrate perfect spherical shapes. An inset in Figure 1d is a feature TEM image of one Au NP, reflecting ultra-smooth surface of particle. Figure 1d is selected area electron diffraction (SAED) pattern of a Au NP in its inset, indicating a face-center cubic (FCC) crystal structure[21]. Additionally, it also reveals that the irradiated Au spherical nanospheres are single crystalline. The average particle size is about 75 (±2.6) nm (Figure 1e), showing an excellent monodispersity with very narrow size distribution. All of the above results confirm that the final Au nanoparticles, obtained by non-focused laser irradiation, are ultra-smooth and perfect spherical shape with a highly single crystalline.

Figure 2 shows the measured absorption spectra of the Au spherical nanoparticle obtained by laser irradiation and pristine Au nanooctahedra dispersed in water. The optical spectra of Au nanospheres and pristine Au nanooctahedra dispersed in water display absorption peaks centered at 542 nm and 578 nm respectively, which originates from the surface plasmon resonances (SPR)[37]. The SPR peak of Au nanoparticle presents a blue-shift after changing their shapes from octahedral to sphere after laser irradiation, meanwhile, the color of colloid solutions changes from light wine reddish to light brick reddish as shown in the inset of Figure 2. The change of SPRs peaks depends extremely on the nanoparticle structures, because the structures with sharp corners induce the inhomogeneous distribution of surface electronic cloud that yielding additional charge separation and different multipolar moments, as reported by Noguez and Katherine[15,38]. When compared with the octahedral structure, the spherical structure of the same size has a blue-shifted peak. It can be attributed to the reduced charge separation in these structures[39]. Once the charge separation decreased, an increasing restoring force is achieved for the dipole oscillation, resulting in a larger frequency and shorter wavelength.

Plasmonic materials, while irradiating with light, can generate plasmon-mediated evanescent fields near their surfaces, which has great potential applications in nanomedicine, nano-optics and plasmonic solar cells[40–42] and so on. Au nanocrystals with controlled shapes, sizes and surfaces, are ideal building blocks for fabrication of plasmonic materials because of their unique and useful optical phenomena, especially for the spherical geometry. Our results reflect that Au uniform octahedral nanoparticles can be prepared by a straightforward polyol-route, and a further laser irradiation is facile, efficient approach to change them into monodispersed Au perfect spherical nanoparticles. Due to their uniform spherical shapes, these Au nanospheres can be self-assembled into hexagonal close-packed monolayer more easily and this monolayer can be further transferred onto a desired substrate. As shown in Figure 3a and 3b, a large-scaled, close-packed periodic array is obtained by a Langmuir-Blodgett technique. The interparticle gap distances of this array are in the range of sub-10 nm, as shown in Fig. S2. Such Au nanosphere array has important applications in areas of surface-enhanced Raman scattering (SERS)[43], catalysis[44] and plasmonic crystals[45], and would render the creation of novel optical materials relying on their tunable plasmonic response[46].

SERS properties of this Au nanosphere arrays on silicon substrates were also investigated. Figure 4a shows the Raman spectra of R6G

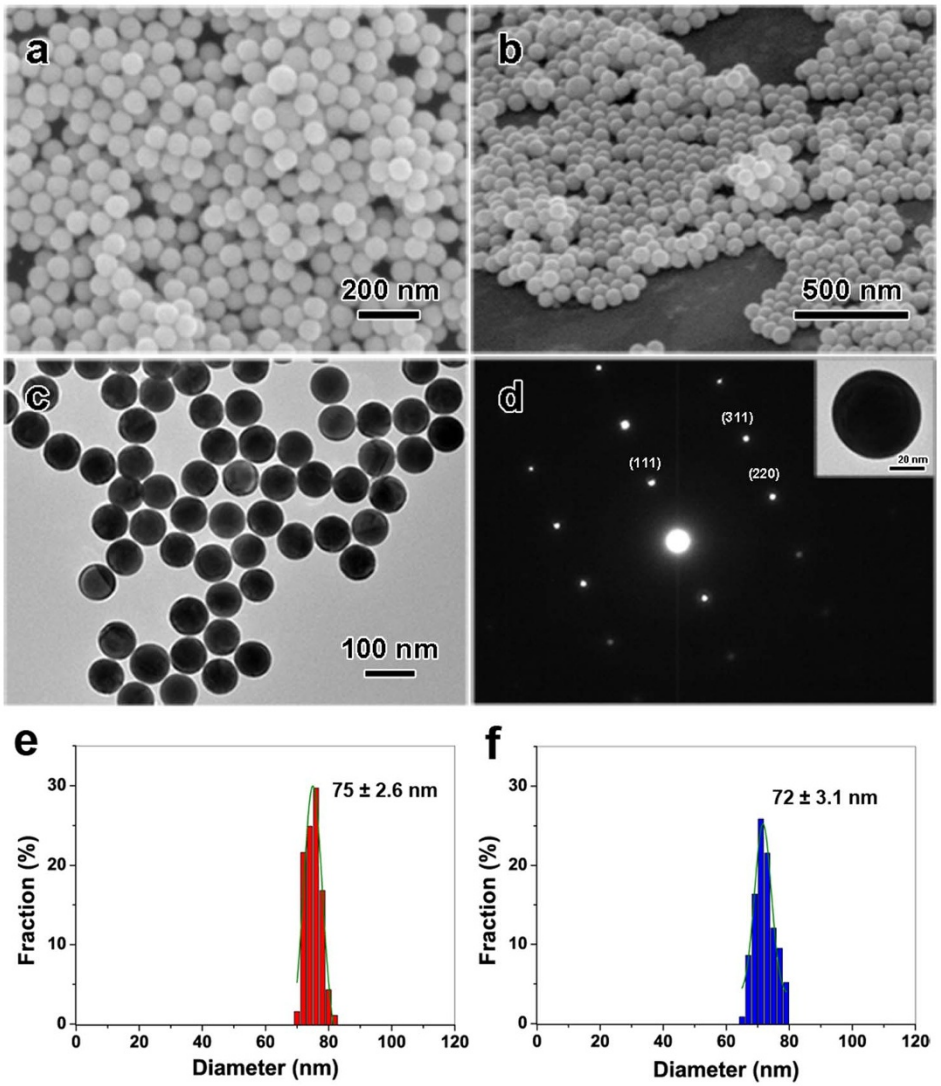

Figure 1 | Au spherical nanoparticles obtained by the non-focused nanosecond pulsed laser irradiation of pristine octahedral nanoparticles (wavelength: 532 nm, fluence: 3.84 mJ cm^{-2}, irradiation time: 60 s). (a) FE-SEM images for top view, and (b) tilted view. (c) A corresponding TEM image. (d) SAED pattern, inset: TEM image of single Au spherical particle. (e) and (f) Size distribution of the spherical and octahedral Au NPs respectively, measured from TEM images of samples with 187 particles: 75 ± 2.6 nm in diameter of Au nanospheres (red column), 72 ± 3.1 nm in edge length of pristine nano-octahedra (blue column).

molecules (10^{-6} M) on the Au nanosphere array (Curve i) and the normal Au film (Curve ii) for comparison. Obviously, the Au nanosphere array exhibits significantly higher SERS performance than that of the simply sputtered Au film. Qualitatively, the Raman counts at 615 cm^{-1} for the Au nanosphere array is about 30 times higher than the normal Au film. When the R6G solution decreased into low concentration (such as 10^{-11} M), the SERS signal is still distinct within 1 s in integral time and 5 mW in laser power, as shown in Figure 4b.

Discussion

The morphological change from nanooctahedra to nanosphere of Au nanoparticle is mainly affected by laser fluence and irradiation time.

Laser fluence. Figure 5 shows the FE-SEM and TEM images of Au NPs obtained by laser irradiation (λ = 532 nm, 20 Hz) at varies of laser fluence for 240 s. The original octahedral nanoparticles display distinct edges and corners with no obvious defects on their surface (Figure 5a and 5b). At a low fluence, for instance, 1.76 mJ cm^{-2}, it is found that octahedral Au NPs can be rarely transformed into spherical shape (Figure 5c and 5d). While increasing the laser fluence to 2.87 mJ cm^{-2}, more than half number of octahera are transformed into spherical shape (Figure 5e and 5f). When the fluence is 3.84 mJ cm^{-2}, a completely spherical shape transformation is achieved (Figure 5g and 5h). If the fluence is too high, a size reduction accompanied with smaller fragments of Au NPs will be witnessed because of the photo-thermal evaporation process[47]. For instance, at the high fluence of 5.50 mJ cm^{-2}, spherical nanoparticles accompanied with small gold cluster are clearly confirmed in the SEM and TEM images (Figure 5i and 5j). These results indicate that the effect of laser fluence is remarkable during laser irradiation and an increase in the laser fluence results in a distinct morphology change from octahedral to spherical at a suitable range of fluence. This can be attributed to the laser-induced surface melting or entire bulk melting of the origin Au NPs after absorbing suitable energy from laser pulses[48]. Besides the shape change during laser irradiation, a fusing process of the Au NPs can be found. This could be the results of the laser-induced agglomeration of two fully melting Au NPs in colloid solution in a little probability, as marked in Figure 5h. In this case, a small quantity

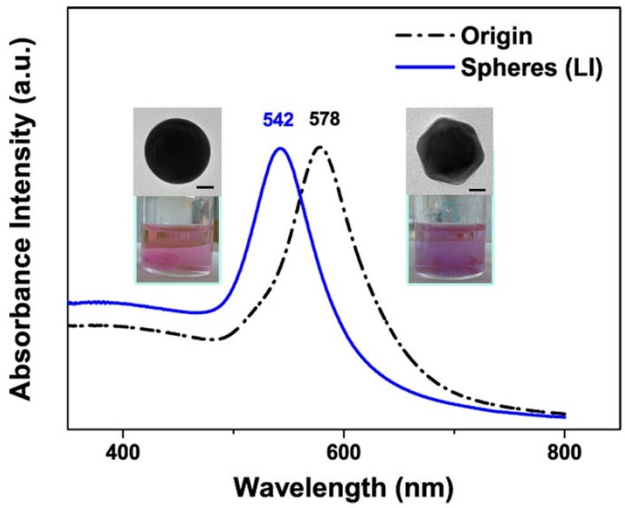

Figure 2 | UV-vis absorption spectra of Au pristine nanooctahedra (black dash dot line) and nanospheres (blue solid line) in water obtained after laser irradiation. Inset: photographs of colloid solution and TEM images of Au nanostructure, and the scale bars are 20 nm.

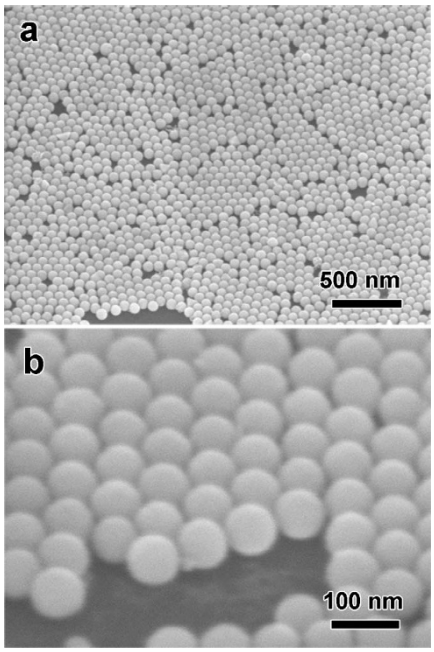

Figure 3 | SEM images of the self-assembled Au monolayer spherical nanoparticle arrays on a silicon substrate. (a) high and (b) low magnification with titled views.

of larger spherical Au particles will be generated from this fusion procedure. Occasionally the intermediate fusing state during fusion can be remained since the quick quenching of the fusing particles in the flowing solution, because this colloid solution keeps vigorously stirring during laser irradiation.

Figure 6 shows the corresponding absorption spectra of Au NPs in DI water irradiated for 240 s at different laser fluences. It indicates that there is a remarkable blue shift in their localized surface plasmon resonances (LSPR) peak with increase of laser fluence due to shape changes of Au nanoparticle (Figure 6a). When Au nanooctahedra is irradiated by laser at 1.76 mJ cm^{-2} for 240 s, the LSPR peak shifts from 578 to 565 nm, which can be attributed to the slight melting of the Au octahedra corner, where the LSPR effect is extremely sensitive[49]. While increasing fluence to 2.87 mJ cm^{-2}, the absorption peak containing a shoulder peak appears. This curve can be divided into two peaks, centered at 540 and 570 nm, which correspond to the LSPR peaks of Au spherical and quasi-octahedral structures, respectively (Figure 6b). When laser fluence increased to 3.84 mJ cm^{-2}, the LSPR peak is shifted into 542 nm because of the complete formation of Au nanospheres. While increasing into a high fluence of 5.50 mJ cm^{-2}, the LSPR peak further shifts to 538 nm due to the size reduction of Au nanospheres. In short, a gentle laser irradiation at 3.84 mJ cm^{-2} can induce completely shape changes from octahedra to sphere and even size reduction, but it is not feasible to obtain a highly monodispersed spherical nanoparticles only by controlling the laser fluence.

According to the above results, there might have two possible routes to tackle this dilemma to prepare monodispersed and perfectly spherical nanoparticles. One is to prolong the irradiation time at lower fluence of 2.87 mJ cm^{-2}, the other is to shorten the irradiation time at higher fluence of 3.84 mJ cm^{-2}. Nonetheless, considering the pulse-to-pulse laser fluctuations, the lower laser fluence (2.87 mJ cm^{-2}) may not be enough to melt the bulk Au NPs completely. Previous studies have pointed out that the high surface-area-to-volume ratio of Au NPs led to a lower surface melting temperature compared to the bulk melting temperature[50]. Thus, the irradiation of low laser fluence produce relatively low temperature and might only induce the surface melting of the Au NPs where the inner core of Au NPs still remains solid state. As shown in Figure 5f, the formation of the partial spherical Au NPs could be the result of the fluctuation of laser pulse, which substantially leads to the particle temperature fluctuating above and below the surface melting temperature. Additionally, prolonging the irradiation time will raise the fusion probability among the melting Au NPs.

Therefore, it is possible to decrease the irradiation time at 3.84 mJ cm^{-2} to prepare monodispersed, Au perfectly spherical nanoparticles. And it will be investigated as following part.

Irradiation time. At fluence of 3.84 mJ cm^{-2} for 240 s, although most of Au nanoparticles are spherical shapes, a few dimer and larger Au nanoparticle turns up during laser irradiation due to fusing of two melted particles, as marked in Figure 5h. These dimer and larger nanoparticles are caused by redundant time of laser irradiation and further increasing the fusion possibility. Figure 7 shows the FE-SEM and TEM images of Au NPs obtained by laser irradiation for varies of decreasing irradiation time at 3.84 mJ cm^{-2}. When increasing the irradiation time gradually, an increasing proportion of spherical Au NPs transformed from Au octahedral nanoparticles was observed, as shown in Figure 7(a–f). Figure 7e and 7f indicate that the expected perfect-spherical Au NPs with highly monodispersity are obtained for laser-irradiation for 60 s. Further prolonging the irradiation time up to 120 s will result in a fusing procedure of the spherical NPs to form Au dimer particles (as marked in Figure 7h). This observation correlated well with our speculation that the fusing of Au NPs is due to the laser irradiation overtime.

We also studied the corresponding absorption spectra of Au NPs at different irradiation time as shown in Figure 8. Figure 8a demonstrates an evolution of blue shift of the absorption spectra varying from 20 to 60 s. When increasing the irradiation time, one can observe that a LSPR peak at 578 nm originated from Au nanooctahedra gradually disappears and an absorption peak at 542 nm caused by Au spherical nanoparticles appears, which corresponds well with the results of the FE-SEM and TEM images. Although further prolonging the irradiation time leads to appearance of a few Au dimer and larger nanoparticles (less than 10% of the total number of Au nanoparticles), the peak position is changed not so much, as depicted in Figure 8b. Therefore, we can conclude that the ultra-spherical Au NPs with highly monodispersity can be achieved only in optimal conditions, that are, gentle laser fluence (3.84 mJ cm^{-2}), proper irradiation time (60 s).

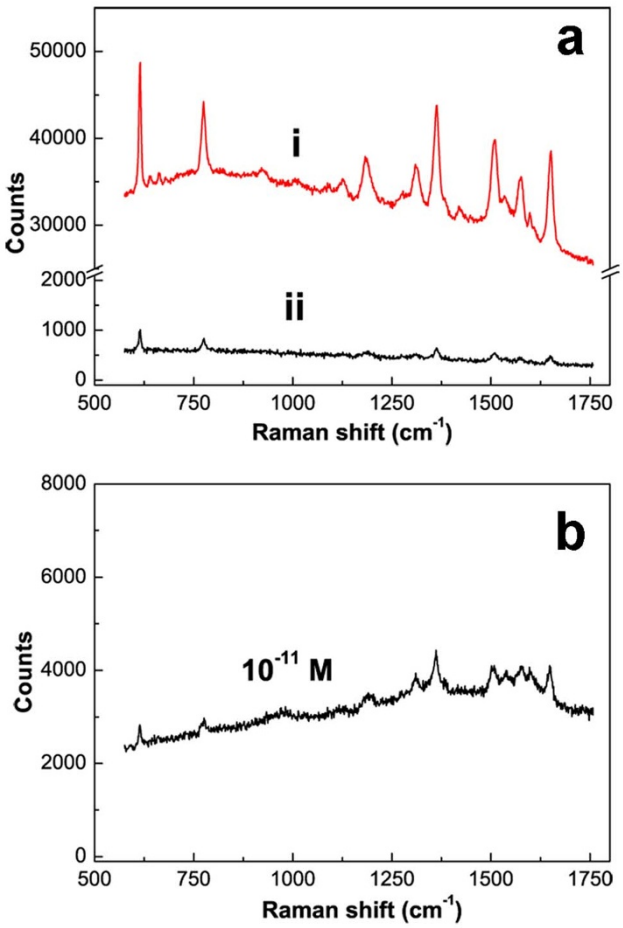

Figure 4 | SERS spectra of R6G molecules on different substrates. (a) after immersion in 10^{-6} mol L^{-1} R6G solution for 30 min (Integral time: 1 s). Curves i: Au spherical nanoparticles array, Curve ii: a normal Au film (about 80 nm in thickness) prepared by sputtering deposition. (b) Raman spectra of R6G molecules on Au nanoparticle array after immersion in 10^{-11} mol L^{-1} R6G solution. Note: the laser powers operated in (a) and (b) are 1 and 5 mW respectively.

Besides above influence factors, a vigorous stir during laser irradiation also affects the formation of high-quality Au nanospheres. It also should be pointed out that the concentration of the colloid solution before laser irradiation should be diluted into a low constant by DI water, because high concentration tends to increase the possibility of collision and fusion among nanoparticles during laser irradiation. Further, to confirm the validity of this method, a similar optimization process was also practiced with the smaller but uniform size of Au nanooctahedra. The ultra-spherical and monodisperse Au NPs with 50 nm in diameter can be obtained by laser irradiation at 3.97 mJ cm^{-2} in laser fluence and 90 s in irradiation times (Fig. S3).

The formation mechanism of Au spherical nanoparticles. In previous studies[51–54], the photothermal evaporation and Coulomb explosion mechanisms are two major models for interpreting the pulse laser-induced size reduction of Au NPs[55–57]. Recently, Werner et. al[58] have demonstrated a clear classification of the photothermal evaporation and coulomb explosion mechanisms based on the two-temperature model (TTM) for simulation. The two-temperature in this model represents for Lattice temperature (T_L) and electron temperature (T_e). They concluded that the photothermal melting-evaporation model is more suitable for the system of nanosecond pulsed-laser excitation. Because, for the gold system, the lattice's melting and boiling temperature (1336 and 3150 K respectively[59]) is easily reached, while leaving the electron temperature (above 7300 K[58]) insufficiently for the coulomb explosion to take place. Accordingly, the photothermal melting-evaporation model is suitable for our work due to application of nanosecond pulsed-laser irradiation and it will lead to a deeper understanding of the mechanism in the morphology transformation of Au NPs. Herein, based on the previous mechanisms presented by Werner et al.[50,58] and Pyatenko et al.[60], we simplify this model to understand the formation mechanism of our work and give as follow.

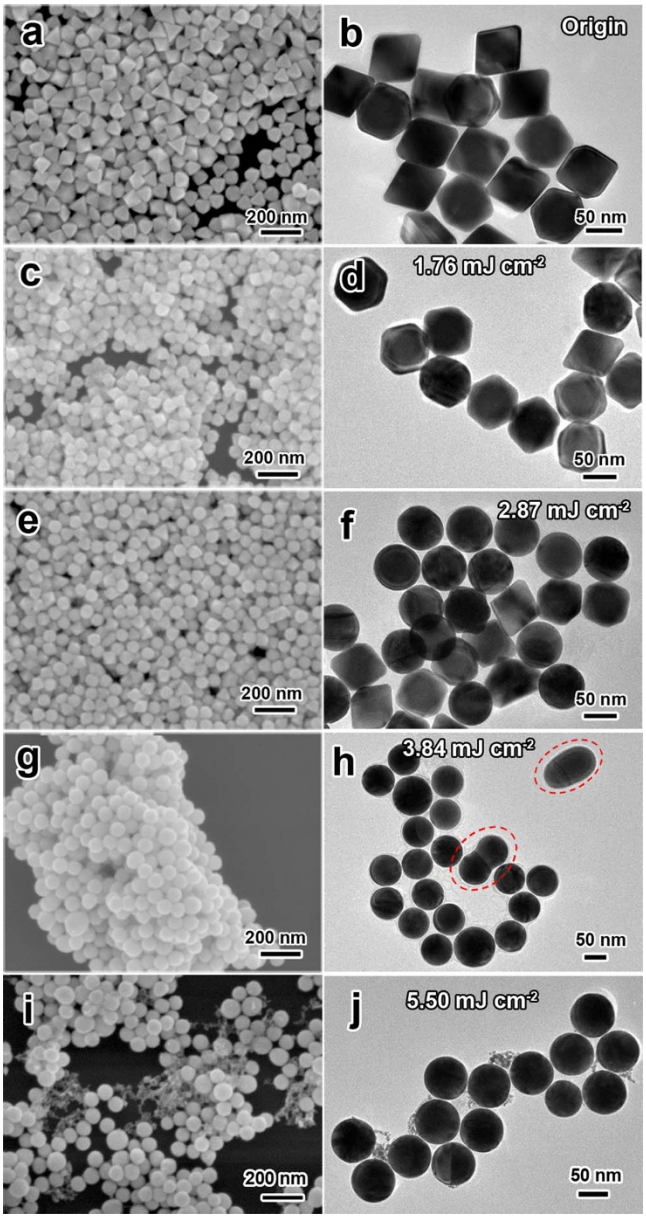

Figure 5 | SEM and TEM images of Au NPs obtained by laser irradiation (λ = 532 nm, 20 Hz) at various laser fluences for 240 s. (a, b) original octahedral nanoparticles, (c, d) 1.76, (e, f) 2.87, (g, h) 3.84 and (i, j) 5.50 mJ cm^{-2}.

A laser energy, E_{abs}, absorbed from an individual pulse of laser beam with pulse energy, $E_0(\tau)$, is equal to[60]

$$E_{abs} = \frac{E_0(\tau)}{S_0}\sigma_{abs}^{\lambda} = J(\tau)\sigma_{abs}^{\lambda} \quad (1)$$

In this equation, beam cross section is S_0, $J(\tau)$ is laser fluence dependent on pulse to pulse time τ, $J(\tau) = E_0(\tau)/S_0$, and σ_{abs}^{λ} is the

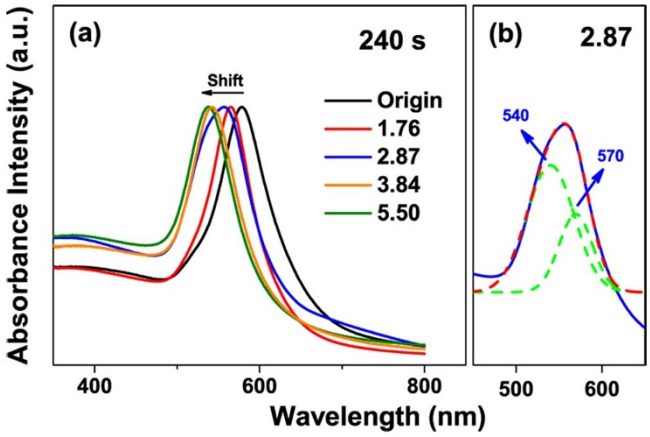

Figure 6 | The absorption spectra of Au NPs in aqueous solution after 532 nm laser irradiation. (a) Different laser fluences for 240 s. (b) Gaussian fitting analysis for the curve of 2.87 mJ cm^{-2}.

particle absorption cross section, which is strongly dependent on laser wavelength and refractive index of surrounding medium n_m. As described in TTM models, the laser energy absorbed by the metal NP is eventually transformed into heat, leading to a rise of the temperatures of T_e, T_L and T_s (surrounding medium). The differential

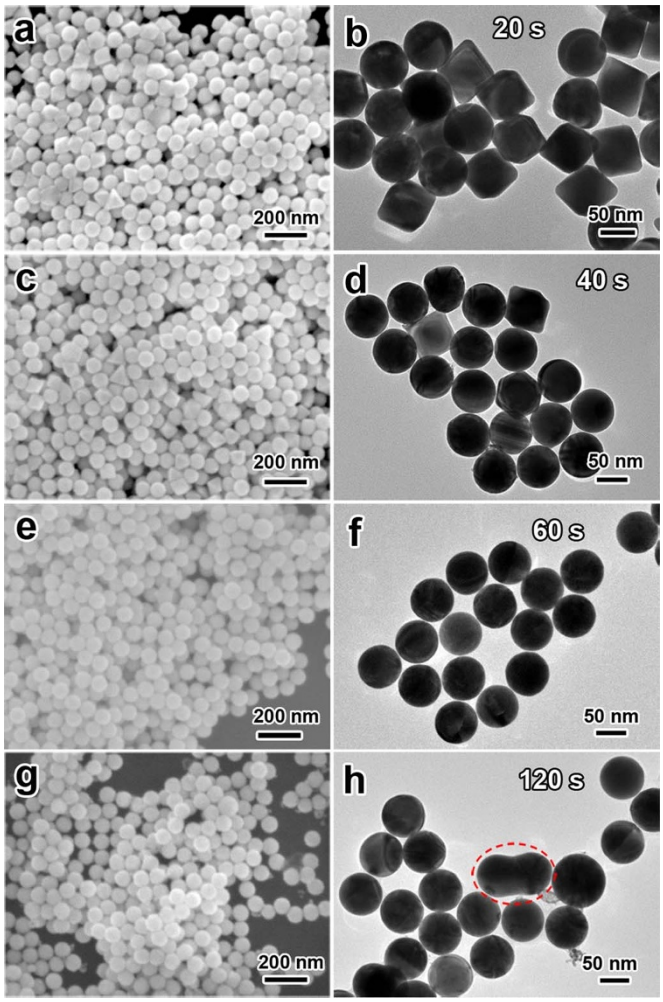

Figure 7 | SEM and TEM images of Au NPs obtained by laser irradiation (λ = 532 nm, 20 Hz) at 3.84 mJ cm^{-2} for (a) 20, (b) 40, (c) 60, and (d) 120 s.

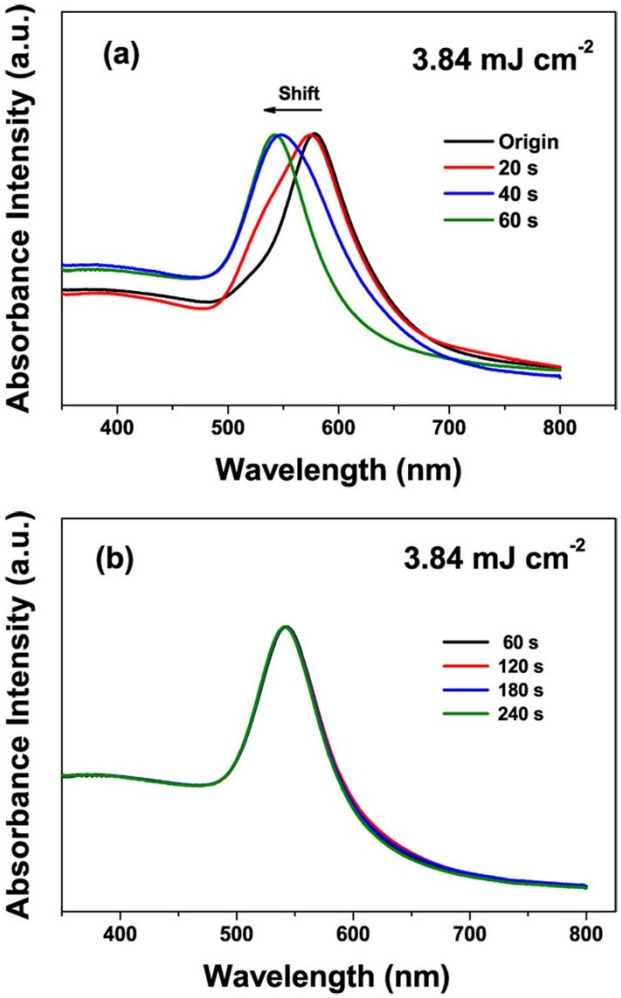

Figure 8 | The absorption spectra of Au NPs obtained by laser irradiation (532 nm, 20 Hz) at 3.84 mJ cm^{-2} for irradiation times varied from (a) 20 s to 60 s, (b) 60 s to 240 s.

heat equation is given as follow[58],

$$m_e \cdot c_e(T_e)\frac{\partial T_e}{\partial \tau} = K_e(T_e, T_L)\cdot\Delta T_e - g(T_e)\cdot[T_e - T_L] + E_{abs} \quad (2)$$

$$m_L \cdot c_L(T_L)\frac{\partial T_L}{\partial \tau} = K_L(T_L)\cdot\Delta T_L + g(T_e)\cdot[T_e - T_L] - F \quad (3)$$

$$m_s \cdot c_s(T_s)\frac{\partial T_s}{\partial \tau} = K_s(T_s)\cdot\Delta T_s + F \quad (4)$$

Here, (m_e, m_L, m_s) and (c_e, c_L, c_s) are the mass and specific heat capacity of the electron, lattice and surrounding medium, respectively; k is the thermal conductivity, Δ represents Laplace operator, g denotes the coefficient of the electron-phonon coupling, E_{abs} is the absorbed laser energy and F represents the interface energy transfer between the NP and liquid. For simplifications, the first terms on the right side of equation (2, 3) are neglected (for $K_e(T_e, T_L)\cdot\Delta T_e$ and $K_L(T_L)\cdot\Delta T_L \approx 0$)[58]. Additionally, for nanosecond laser excitation, the time evolution of T_e and T_L is in quasi-equilibrium ($T_L \approx T_e$) during the excitation period[58], and the mass of electron could be negligible compared with the one of lattice. For convenience, the heat loss caused by the radiation cooling and heat diffusion to the surrounding water (F) is also negligible during particle heating, because the typical times needed for particle cooling/solidification range

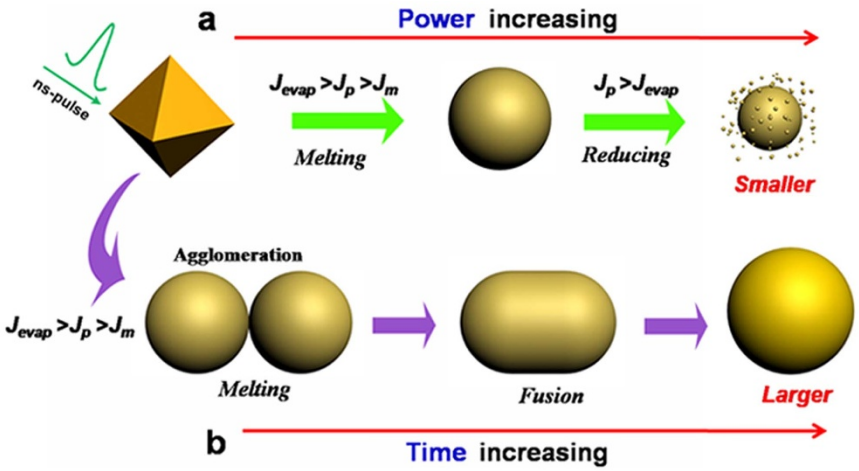

Figure 9 | Schematic illustration of nanosecond laser-irradiation induced shape transformation of the octaheral Au NPs in water. J_m, threshold for melting to liquid phase of bulk gold; J_{evp}, threshold for boiling to evaporation of bulk gold; J_p, laser fluence acting on gold NPs.

from 10^{-5} to 10^{-6} s[60], which are much longer than the nanosecond laser ($\tau_p = 10^{-8}$ s). On the other hand, the lattice heat will not be accumulated from one laser pulse to the next, for the time required for the cooling/solidification of Au NP is much shorter than 50 ms (20 Hz). According to the above approximation, the equations (2–4) will be generalized into a simplified form during the particle heating process. Integrated with the equation (1), the general relationship between the nanoparticle temperatures (T) and laser fluences (J) is given in equation (5).

$$J_j \cdot \sigma_{abs}^{\lambda} = m_p \cdot \int_{T_0}^{T} c_p^i(T) \cdot d(T) = m_p \sum H_i;\ for\ i \in (0, j) \qquad (5)$$

Where, the subscript j defines as a mathematic set of the particle thermodynamic states, e.g. heating, melting and boiling to evaporation. H is the relative enthalpy per unit mass. Herein, the laser fluence (J) for each laser pulse can be considered as a constant. It is thought that a high absorption cross section σ_{abs}^{λ} is achieved at 532 nm exciting because of the SPR property of Au NPs. When adopting the laser beam with wavelength of 532 nm, σ_{abs}^{λ} is also a constant value since the octahedral Au NPs employed in our research are uniform and highly monodispersed.

With the help of equation (5), it is easy to understand the mechanism of the photothermal melting-evaporation of shape changes from Au nanooctahedron to nanosphere under nanosecond pulsed-laser irradiation. Figure 9 shows a schematic to illustrate the morphological evolution of the octahedral Au NPs under nanosecond pulsed-laser irradiation. When laser fluence J_p is smaller than the bulk melting threshold J_m, only particle heating is achieved or even a slight melting sharp corner is taken place. Or perhaps a surface melting of particles will be achieved due to their high surface-area-to-volume ratio[61]. While at the condition of $J_m < J_P < J_{evp}$, a bulk melting occurs and the particle turns into ultra-spherical liquid phase. Once the heat dissipation to the surrounding medium, particles solidify into ultra-spherical phase for keeping. However, when the condition of $J_P > J_{evp}$ is met, the particle reaches the boiling temperature and starts to evaporate. The laser-induced size reduction takes place, and the slightly smaller and much smaller Au NPs are observed as a result of the layer-by-layer surface evaporation.

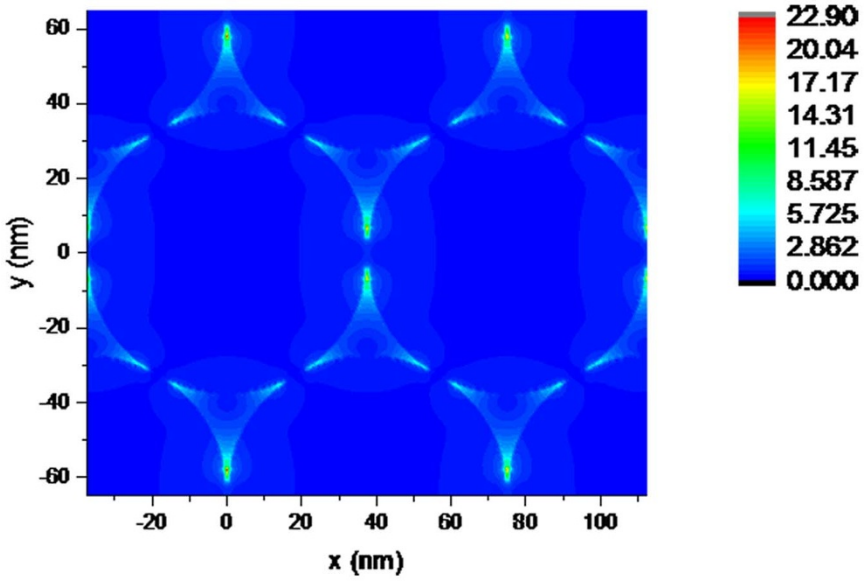

Figure 10 | FDTD simulation of electric-field intensity distribution (indicated by the color bar) of Au nanosphere array by self-assembly. Parameters were based on those of the Au nanosphere array with hexagonal-close-packed arrangement, a periodicity is 75 nm, the substrate is silicon and the excitation line is 532 nm.

A large scale ultra-spherical and highly monodispersed Au NPs can be prepared via this two-step strategy at optimal conditions. However, a small quantity of spherical Au NPs will agglomerate and fuse into a larger spherical NPs for the overtime laser irradiation, as evidenced from the TEM image of Figure 5h and 7h. Therefore, the interaction among the spherical Au NPs should be taken into consideration during laser irradiation. According to Takeshi et al.'s previous research[62], laser irradiation using a non-focused laser beam will bring about the removal and decomposition of stabilizing molecules on the surface of the Au NPs, and that causes the agglomeration of NPs dynamically, then induces the fusion of the agglomerated Au NPs. In our work, a small quantity of the Au nanospheres obtained by laser irradiation also displays a tendency to agglomerate into dimer dynamically. While irradiated by the next laser pulse, the dimer turns to a bulk melting state and dynamically fusing into a larger spherical particle, as illustrated in Figure 9b. This aggolomeration of Au Nanospheres can be explained for the partial removal and decomposition of PDDA molecules on the surface of Au NPs during laser irradiation. In that case, prolonging the irradiation time will set up a vicious circle of the fusion process. In such vicious circle, larger gold nanospheres are gathering increase and lead to a poor monodispersity. Therefore, we confirm that an appropriate irradiation time is essential to maintain the monodisperity of Au nanospheres while the phase transformation takes place.

SERS active substrate of Au periodic nanosphere array. Finite-Difference Time-Domain (FDTD) simulation was employed to fully understand local electric field distribution of Au nanosphere array under light excitation, as shown in Figure 10. As we all know, two mechanism models, electromagnetic (EM) enhancement and chemical enhancement (CE), are the predominant roles in explaining the SERS phenomenon[63]. From the EM point of view, when the frequency of incident light is resonant with the SPR of the Au nanoparticle, a redistribution of the local EM field is induced by the coherent action between their dipolar filed and the exciting electric field. This process leads to a special 'hot spot' position, in which the EM field around the NP is greatly enhanced. The molecule near or adsorbed at the hot spot is excited and results in much enhanced Raman-scattered signals. What's more, gaps (in sub-10 nm range) between adjacent Au nanoparticles provided further enhanced local EM fields because of the electromagnetic coupling at the junctions between neighboring nanoparticles[43]. This interparticle electromagnetic coupling causes the amplification of the polarization of the plasmons, thus generating large enhancement SERS signal from molecules in illuminated area, known as 'hot spots'. Herein, the periodic NP arrays results from self-assembly provide maximum surface density of well-defined "hot spots" upon optical excitation, exhibit enormous near-field enhancements exploitable for large SERS enhancements.

In conclusion, a facile and effective strategy is developed to synthesize monodispersed Au spherical nanoparticles by two steps, preparation of large-scale monocrystalline Au nanooctahedra with uniform size by a polyol-route and subsequently rapid synthesis of monodispersed Au nanospheres through a laser irradiation-induced shape conversion of Au nanooctahedra in a liquid under ambient atmosphere. High monodispersed, ultra-smooth gold nanospheres can be obtained by simply optimizing the laser fluence and irradiation time. We discovered that there have two major parameters that affect the formation quality of Au nanospheres: laser fluence and irradiation time. Mechanism investigation suggests that photothermal melting-evaporation model is suitable for the system of nanosecond pulsed-laser excitation to understand the complex process in our work. These Au nanoparticles could be fabricated into periodic monolayer arrays by self-assembly utilizing their high monodispersity and perfect spherical shape. These Au nanospheres arrays demonstrated very good SERS enhancement related to their periodic structure due to existence of many SERS hot spots between neighboring Au nanospheres in an array and hence can be used as an excellent and promising candidate for sensing and spectroscopic enhancement, catalysis, energy, and biology.

Methods

Uniform Au octahedral nanocrystals were prepared by a facile polyol route according to our previous work[37]. Briefly, a given amount of chloroauric acid ($HAuCl_4$, Aldrich) as gold source, poly(diallyldimethylammonium) chloride (PDDA, M_w = 100,000 ~ 200,000, 20 wt % in H_2O, Aldrich) as surfactant, and HCl solution (Aldrich) were introduced into an ethylene glycol solution in a glass vial under vigorous stir. The final concentration of $AuCl_4^-$ ions, PDDA, and HCl in the initial gold precursor was 0.5 mM, 25 mM, and 5 mM, respectively. Finally, the mixture solution was heated at 195°C for 30 min in an oil bath without stir. The final color of the solution appears to light wine reddish, reflecting the formation of Au nanocrystals.

The colloidal Au octahedral nanoparticle diluted with deionized (DI) water (1 : 3 volume ratios, 4 mL in total) was added into a clean weighing bottle (25 mm × 40 mm) under magnetic blender. A non-focused Nd: YAG laser operated at 20 Hz with a wavelength of 532 nm and pulse duration of 10 ns vertically irradiated into the Au colloidal solution in weighing bottle. The diameter of laser beam irradiated on the solution was about 5 mm. The solution was continuously stirred by magnetic rotor during irradiation. With increase of irradiation time, the color of colloidal Au nanoparticle was gradually changed from light wine reddish to light brick reddish. The final product was collected by centrifugation at 12, 000 rpm for 45 min and washed repeatedly with pure DI water for further characterization and optical property study. These Au nanospheres obtained by laser irradiation were modified with excess amounts of 30 mM dodecanethiol in ethanol solution as the capping agent for further self-assembly[64] and then centrifuged, dispersed into chloroform. The Au monolayer nanosphere arrays were formed by dropping the mixed solution onto the water surface by self-assembling process until the chloroform was fully evaporated. This Au monolayer was gently picked up by using a clear silicon substrate, dried with flowing N_2 gas, and then placed into a ultra-violet ozone cleaning systems (UVOCS) for 1 h to remove the surface coating materials. For Raman spectral examination, these pretreated samples were soaked into Rhodamine 6G (R6G) with different concentrations for 30 min, rinsed with DI water, and dried with flowing N_2 gas for further SERS characterization.

The morphology of the final product was characterized by a field emission scanning electron microscopy (FE-SEM, FEI Sirion 200). The samples for TEM examination were prepared by dropping the Au nanoparticle colloidal solution on copper grids with thin carbon coating and then drying by evaporation in air at room temperature, selected area electron diffraction (SAED) studies were performed on a JEM-200CX operated at 200 kV. For optical measurement, the products were dispersed in water and then optical absorption spectra were recorded with a spectrophotometer (Cary 500) in the wavelength range of 200–800 nm, using an optical quartz cell with a 10 mm path-length. The Raman spectra were recorded on a macroscopic confocal Raman spectroscopy (LAICA DM 2500) by using a laser beam 532 nm in wavelength for excitation at room temperature. The integral time and accumulations were 1 s and 3 times for all samples respectively.

1. Howes, P. D., Rana, S. & Stevens, M. M. Plasmonic nanomaterials for biodiagnostics. *Chem. Soc. Rev.* **43**, 3835–3853 (2014).
2. Dykman, L. A. & Khlebtsov, N. G. Uptake of Engineered Gold Nanoparticles into Mammalian Cells. *Chem. Rev.* **114**, 1258–1288 (2013).
3. Giljohann, D. A. *et al.* Gold nanoparticles for biology and medicine. *Angew. Chem. Int. Ed.* **49**, 3280–3294 (2010).
4. Tokel, O., Inci, F. & Demirci, U. Advances in Plasmonic Technologies for Point of Care Applications. *Chem. Rev.* **114**, 5728–5752 (2014).
5. Dreaden, E. C. *et al.* The golden age: gold nanoparticles for biomedicine. *Chem. Soc. Rev.* **41**, 2740–2779 (2012).
6. Murphy, C. J. *et al.* Gold nanoparticles in biology: beyond toxicity to cellular imaging. *Accounts Chem. Res.* **41**, 1721–1730 (2008).
7. Jin, R. C. *et al.* Controlling anisotropic nanoparticle growth through plasmon excitation. *Nature* **425**, 487–490 (2003).
8. Daniel, M.-C. & Astruc, D. Gold nanoparticles: assembly, supramolecular chemistry, quantum-size-related properties, and applications toward biology, catalysis, and nanotechnology. *Chem. Rev.* **104**, 293–346 (2004).
9. Hu, M. *et al.* Gold nanostructures: engineering their plasmonic properties for biomedical applications. *Chem. Soc. Rev.* **35**, 1084–1094 (2006).
10. Kelly, K. L., Coronado, E., Zhao, L. L. & Schatz, G. C. The optical properties of metal nanoparticles: the influence of size, shape, and dielectric environment. *J. Phys. Chem. B* **107**, 668–677 (2003).
11. Jain, P. K., Lee, K. S., El-Sayed, I. H. & El-Sayed, M. A. Calculated absorption and scattering properties of gold nanoparticles of different size, shape, and composition: Applications in biological imaging and biomedicine. *J. Phys. Chem. B* **110**, 7238–7248 (2006).
12. Ciracì, C. *et al.* Probing the ultimate limits of plasmonic enhancement. *Science* **337**, 1072–1074 (2012).
13. Luk'yanchuk, B. *et al.* The Fano resonance in plasmonic nanostructures and metamaterials. *Nat. Mater.* **9**, 707–715 (2010).
14. Bachelier, G. *et al.* Fano profiles induced by near-field coupling in heterogeneous dimers of gold and silver nanoparticles. *Phys. Rev. Lett.* **101**, 197401 (2008).

15. Noguez, C. Surface plasmons on metal nanoparticles: the influence of shape and physical environment. *J. Phys. Chem. C* **111**, 3806–3819 (2007).
16. Albanese, A., Tang, P. S. & Chan, W. C. The effect of nanoparticle size, shape, and surface chemistry on biological systems. *Annu. Rev. Biomed. Eng.* **14**, 1–16 (2012).
17. Cho, E. C., Au, L., Zhang, Q. & Xia, Y. The effects of size, shape, and surface functional group of gold nanostructures on their adsorption and internalization by cells. *Small* **6**, 517–522 (2010).
18. Chithrani, B. D., Ghazani, A. A. & Chan, W. C. Determining the size and shape dependence of gold nanoparticle uptake into mammalian cells. *Nano Lett.* **6**, 662–668 (2006).
19. Chithrani, B. D. & Chan, W. C. Elucidating the mechanism of cellular uptake and removal of protein-coated gold nanoparticles of different sizes and shapes. *Nano Lett.* **7**, 1542–1550 (2007).
20. Lu, F. *et al.* Truncated ditetragonal gold prisms as nanofacet activators of catalytic platinum. *J. Am. Chem. Soc.* **133**, 18074–18077 (2011).
21. Personick, M. L. & Mirkin, C. A. Making Sense of the Mayhem behind Shape Control in the Synthesis of Gold Nanoparticles. *J. Am. Chem. Soc.* **135**, 18238–18247 (2013).
22. Lee, Y.-J. *et al.* Ultra-Smooth, Highly Spherical Monocrystalline Gold Particles for Precision Plasmonics. *ACS nano* **7**, 11064–11070 (2013).
23. Ji, X. *et al.* Size control of gold nanocrystals in citrate reduction: the third role of citrate. *J. Am. Chem. Soc.* **129**, 13939–13948 (2007).
24. Bastús, N. G., Comenge, J. & Puntes, V. Kinetically controlled seeded growth synthesis of citrate-stabilized gold nanoparticles of up to 200 nm: size focusing versus Ostwald ripening. *Langmuir* **27**, 11098–11105 (2011).
25. Shimizu, T., Teranishi, T., Hasegawa, S. & Miyake, M. Size evolution of alkanethiol-protected gold nanoparticles by heat treatment in the solid state. *J. Phys. Chem. B* **107**, 2719–2724 (2003).
26. Liz-Marzan, L. M. Gold nanoparticle research before and after the Brust-Schiffrin method. *Chem. Commum.* **49**, 16–18 (2013).
27. Jana, N. R., Gearheart, L. & Murphy, C. J. Seeding growth for size control of 5–40 nm diameter gold nanoparticles. *Langmuir* **17**, 6782–6786 (2001).
28. Jana, N. R., Gearheart, L. & Murphy, C. J. Seed-mediated growth approach for shape-controlled synthesis of spheroidal and rod-like gold nanoparticles using a surfactant template. *Adv. Mater.* **13**, 1389 (2001).
29. Wang, H. *et al.* General Bottom-Up Construction of Spherical Particles by Pulsed Laser Irradiation of Colloidal Nanoparticles: A Case Study on CuO. *Chem. Eur. J.* **18**, 163–169 (2012).
30. Swiatkowska-Warkocka, Z. *et al.* Pulsed laser irradiation of colloidal nanoparticles: a new synthesis route for the production of non-equilibrium bimetallic alloy submicrometer spheres. *RSC Adv.* **3**, 79–83 (2013).
31. Tsuji, T. *et al.* Fabrication of Spherical-Shaped Submicron Particles of ZnO Using Laser-induced Melting of Submicron-sized Source Materials. *J. Laser Micro Nanoen.* **8**, 292–295 (2013).
32. Wang, H. *et al.* Photomediated assembly of single crystalline silver spherical particles with enhanced electrochemical performance. *J. Mater. Chem. A* **1**, 692–698 (2013).
33. Werner, D. & Hashimoto, S. Controlling the Pulsed-Laser-Induced Size Reduction of Au and Ag Nanoparticles via Changes in the External Pressure, Laser Intensity, and Excitation Wavelength. *Langmuir* **29**, 1295–1302 (2013).
34. Saha, K. *et al.* Gold nanoparticles in chemical and biological sensing. *Chem. Rev.* **112**, 2739–2779 (2012).
35. Cho, E. C., Au, L., Zhang, Q. & Xia, Y. N. The Effects of Size, Shape, and Surface Functional Group of Gold Nanostructures on Their Adsorption and Internalization by Cells. *Small* **6**, 517–522 (2010).
36. Jain, P. K., El-Sayed, I. H. & El-Sayed, M. A. Au nanoparticles target cancer. *nano today* **2**, 18–29 (2007).
37. Li, C. *et al.* A facile polyol route to uniform gold octahedra with tailorable size and their optical properties. *ACS nano* **2**, 1760–1769 (2008).
38. Willets, K. A. & Van Duyne, R. P. Localized surface plasmon resonance spectroscopy and sensing. *Annu. Rev. Phys. Chem.* **58**, 267–297 (2007).
39. Cobley, C. M. *et al.* Controlled etching as a route to high quality silver nanospheres for optical studies. *J. Phys. Chem. C* **113**, 16975–16982 (2009).
40. Murray, W. A. & Barnes, W. L. Plasmonic materials. *Adv. Mater.* **19**, 3771–3782 (2007).
41. Pelton, M., Aizpurua, J. & Bryant, G. Metal-nanoparticle plasmonics. *Laser Photonics Rev.* **2**, 136–159 (2008).
42. Giannini, V., Fernandez-Dominguez, A. I., Heck, S. C. & Maier, S. A. Plasmonic nanoantennas: fundamentals and their use in controlling the radiative properties of nanoemitters. *Chem. Rev.* **111**, 3888–3912 (2011).
43. Wang, H., Levin, C. S. & Halas, N. J. Nanosphere arrays with controlled sub-10-nm gaps as surface-enhanced Raman spectroscopy substrates. *J. Am. Chem. Soc.* **127**, 14992–14993 (2005).
44. Xia, H. & Wang, D. Fabrication of Macroscopic Freestanding Films of Metallic Nanoparticle Monolayers by Interfacial Self-Assembly. *Adv. Mater.* **20**, 4253–4256 (2008).
45. Tao, A. R. *et al.* Self-Organized Silver Nanoparticles for Three-Dimensional Plasmonic Crystals. *Nano Lett.* **8**, 4033–4038 (2008).
46. Lin, M.-H., Chen, H.-Y. & Gwo, S. Layer-by-layer assembly of three-dimensional colloidal supercrystals with tunable plasmonic properties. *J. Am. Chem. Soc.* **132**, 11259–11263 (2010).
47. Inasawa, S., Sugiyama, M., Noda, S. & Yamaguchi, Y. Spectroscopic study of laser-induced phase transition of gold nanoparticles on nanosecond time scales and longer. *J. Phys. Chem. B* **110**, 3114–3119 (2006).
48. Werner, D., Hashimoto, S. & Uwada, T. Remarkable Photothermal Effect of Interband Excitation on Nanosecond Laser-Induced Reshaping and Size Reduction of Pseudospherical Gold Nanoparticles in Aqueous Solution. *Langmuir* **26**, 9956–9963 (2010).
49. Wang, Y. *et al.* Synthesis of Silver Octahedra with Controlled Sizes and Optical Properties via Seed-Mediated Growth. *ACS nano* **7**, 4586–4594 (2013).
50. Werner, D., Furube, A., Okamoto, T. & Hashimoto, S. Femtosecond Laser-Induced Size Reduction of Aqueous Gold Nanoparticles: In Situ and Pump−Probe Spectroscopy Investigations Revealing Coulomb Explosion. *J. Phys. Chem. C* **115**, 8503–8512 (2011).
51. Shoji, M., Miyajima, K. & Mafune, F. Ionization of gold nanoparticles in solution by pulse laser excitation as studied by mass spectrometric detection of gold cluster ions. *J. Phys. Chem. C* **112**, 1929–1932 (2008).
52. Takami, A., Kurita, H. & Koda, S. Laser-induced size reduction of noble metal particles. *J. Phys. Chem. B* **103**, 1226–1232 (1999).
53. Giammanco, F., Giorgetti, E., Marsili, P. & Giusti, A. Experimental and theoretical analysis of photofragmentation of Au nanoparticles by picosecond laser radiation. *J. Phys. Chem. C* **114**, 3354–3363 (2010).
54. Valev, V. K. *et al.* Plasmon-Enhanced Sub-Wavelength Laser Ablation: Plasmonic Nanojets. *Adv. Mater.* **24**, OP29–OP35 (2012).
55. Yang, G. W. Laser ablation in liquids: Applications in the synthesis of nanocrystals. *Prog. Mater. Sci.* **52**, 648–698 (2007).
56. Zeng, H. *et al.* Nanomaterials via laser ablation/irradiation in liquid: a review. *Adv. Funct. Mater.* **22**, 1333–1353 (2012).
57. Plech, A. *et al.* Laser-induced heating and melting of gold nanoparticles studied by time-resolved x-ray scattering. *Phys. Rev. B* **70**, 195423 (2004).
58. Werner, D. & Hashimoto, S. Improved working model for interpreting the excitation wavelength-and fluence-dependent response in pulsed laser-induced size reduction of aqueous gold nanoparticles. *J. Phys. Chem. C* **115**, 5063–5072 (2010).
59. Meshcheryakov, Y. P. & Bulgakova, N. Thermoelastic modeling of microbump and nanojet formation on nanosize gold films under femtosecond laser irradiation. *Appl. Phys. A* **82**, 363–368 (2006).
60. Pyatenko, A., Wang, H., Koshizaki, N. & Tsuji, T. Mechanism of pulse laser interaction with colloidal nanoparticles. *Laser Photonics Rev.* **7**, 596–604 (2013).
61. Link, S., Wang, Z. L. & El-Sayed, M. A. How Does a Gold Nanorod Melt? *J. Phys. Chem. B* **104**, 7867–7870 (2000).
62. Tsuji, T. *et al.* Preparation and investigation of the formation mechanism of submicron-sized spherical particles of gold using laser ablation and laser irradiation in liquids. *Phys. Chem. Chem. Phys.* **15**, 3099–3107 (2013).
63. Wang, Y., Yan, B. & Chen, L. SERS tags: novel optical nanoprobes for bioanalysis. *Chem. Rev.* **113**, 1391–1428 (2012).
64. Bigioni, T. P. *et al.* Kinetically driven self assembly of highly ordered nanoparticle monolayers. *Nat. Mater.* **5**, 265–270 (2006).

Acknowledgments

The authors acknowledge the financial support from the National Basic Research Program of China (Grant No. 2012CB932303), Recruitment Program of Global Experts (C), Natural Science Foundation of China (Grant Nos. 51371165, 21103068), Cross-disciplinary Collaborative Teams and CAS/SAFEA International Partnership Program for Creative Research Teams. C. Li as a Taishan Scholar Endowed Professor acknowledges the supports from Shandong province and UJN.

Author contributions

Y.L. proposed and supervised the project. D.L., T.Z. and C.L. carried out experiments. C.W., G.D., X.L. and H.Z. contributed reagents/analytic tools. D.L., Y.L., C.L. and F.Z. analyzed date. D.L., Y.L. and C.L. wrote the main manuscript text.

Additional information

Supplementary information accompanies this paper at http://www.nature.com/scientificreports

Competing financial interests: The authors declare no competing financial interests.

How to cite this article: Liu, D. *et al.* Rapid Synthesis of Monodisperse Au Nanospheres through a Laser Irradiation -Induced Shape Conversion, Self-Assembly and Their Electromagnetic Coupling SERS Enhancement. *Sci. Rep.* **5**, 7686; DOI:10.1038/srep07686 (2015).